COBEM 2021 26th International Congress of Mechanical Engineering
ABCM Associação Brasileira de Engenharia e Ciências Mecânicas
November 22-26, 2021, Virtual Congress, Brazil

COB-2021-1016
Lyapunov-Based Control Design for a Fully-Actuated Non-Planar Hexa-Rotor Aerial Vehicle

José Agnelo Bezerra [1]
Davi A. Santos [2]

Instituto Tecnológico de Aeronáutica
Praça Marechal Eduardo Gomes, 50
São José dos Campos/SP - Brasil
[1] agnelo@ita.br, [2] davists@ita.br

Abstract. *This paper is concerned with the attitude and position control of a fully-actuated multirotor aerial vehicle (MAV) equipped with six reversible fixed rotors in a non-planar configuration. The complete nonlinear dynamics of the vehicle is modeled in a state error formulation with six degrees-of-freedom (DOF), being three for position and three others for attitude, while the control input is also a six-DOF variable described by the resultant force and torque acting on the system. A control law is designed using the Lyapunov direct method, which ensures global asymptotic stability for both closed-loop translational and rotational dynamics. Therefore, we can obtain a controller which employs inverse dynamics to compensate the nonlinear terms of the plant, and contains proportional-derivative control actions, allowing easy tuning and implementation in practical MAV applications. The proposed control law is evaluated and demonstrated in a software-in-the-loop simulator, which shows its effectiveness to stabilize all the hexa-rotor states.*

Keywords: *multirotor aerial vehicle, nonlinear control*

1. INTRODUCTION

Multirotor aerial vehicles (MAVs) have been employed in an increasing number of civilian applications and, for the near future, intensive use of them in urban areas is expected, performing missions such as air transportation, delivery of goods, and aerial manipulation. These tasks demand in general a high level of maneuverability, thus they are most indicated for vehicles with independent dynamics of position and attitude. Such fully-actuated MAVs can be equipped with fixed or vectorable rotors in one or two degrees-of-freedom (DOF), which leads to a sophisticated control problem.

Several prototypes of fully-actuated MAVs have already been proposed. The papers Ryll *et al.* (2012); Segui-Gasco *et al.* (2013); Oosedo *et al.* (2016) have analyzed some quad-rotor designs with vectorable rotors. In Kamel *et al.* (2018), a hexa-rotor equipped with one-DOF vectorable rotors has been presented, while Crowther *et al.* (2011); Rajappa *et al.* (2015); Park *et al.* (2016) have proposed hexa-rotor designs with tilted fixed rotors. Differently, the paper Ryll *et al.* (2016) has studied a morphing hexa-rotor that can change between an under-actuated and a fully-actuated configuration. Finally, an octa-rotor with fixed rotors in a non-planar configuration has been presented in Brescianini and D'Andrea (2016). All the above-cited references have employed independent inverse-dynamics control laws with PID actions for the position and attitude dynamics. However, none of the papers have analyzed the stability of the closed-loop system.

This paper proposes a six-DOF inverse-dynamics control law with proportional-derivative actions for the complete dynamics of a fully-actuated MAV. The controller is applied to a novel hexa-rotor design, which counts with tilted fixed rotors in a non-planar configuration. Using state-error modeling for the vehicle's closed-loop dynamics, we present a detailed stability analysis based on the direct method of Lyapunov, differently from all the cited references. Therefore, we can show that the proposed controller ensures global asymptotic stability for any state condition.

The remaining text is organized in the following manner. Section 2. presents the hexa-rotor modeling and defines the control problem. Section 3. designs the proposed control law and analyzes the closed-loop stability. Section 4. presents the simulation results. Finally, Section 5. concludes the paper.

2. PROBLEM STATEMENT

This section is organized as follows: Subsection 2.1 describes the adopted notation; Subsection 2.2 presents the rotor configuration of the considered hexa-rotor; Subsection 2.3 deals with the MAV dynamic modeling; and Subsection 2.4 enunciates the MAV control problem.

2.1 Notation

The set of (non-negative) real numbers is denoted by $\mathbb{R}$ ($\mathbb{R}_+$). Scalar quantities are denoted by lowercase italic letters, *e.g.*, $v \in \mathbb{R}$. Vector quantities are represented by lowercase boldface letters, *e.g.*, $\mathbf{v} \in \mathbb{R}^n$, and matrices with arbitrary dimensions are represented by uppercase boldface letters, *e.g.*, $\mathbf{A} \in \mathbb{R}^{n\times m}$. An algebraic vector can be described by $\mathbf{v} = (v_1, v_2, \ldots, v_n)$, where $v_i, \forall i \in \{1, 2, \ldots, n\}$, are its components. The time dependency of any quantity (*e.g*, $\mathbf{v} = \mathbf{v}(t)$) will be generally omitted. The transpose of a matrix $\mathbf{A}$ is denoted by $\mathbf{A}^{\mathrm{T}}$. The $n \times n$ identity matrix is denoted by $\mathbf{I}_n$, while $n \times m$ zero matrices are denoted by $\mathbf{0}_{n\times m}$. Coordinate-free geometric (or physical) vectors are denoted as $\vec{v}$, while versors (with unit magnitude) are denoted as $\hat{v}$. Cartesian coordinate systems (CCSs) are denoted as $\mathcal{S}_b \triangleq \{B; \hat{x}_b, \hat{y}_b, \hat{z}_b\}$, where B represents its origin and the versors $\hat{x}_b$, $\hat{y}_b$, and $\hat{z}_b$ form an orthonormal basis for the three-dimensional space. The algebraic vector resulting from the projection of $\vec{v}$ onto $\mathcal{S}_b$ is represented by $\mathbf{v}_b \in \mathbb{R}^3$, which is referred to as the $\mathcal{S}_b$ representation of $\vec{v}$. The canonical basis for $\mathbb{R}^3$ is represented by the vectors $\mathbf{e}_1 \triangleq (1, 0, 0)$, $\mathbf{e}_2 \triangleq (0, 1, 0)$, and $\mathbf{e}_3 \triangleq (0, 0, 1)$. The attitude matrix that represents the orientation of $\mathcal{S}_b$ w.r.t. $\mathcal{S}_a$ is denoted by $\mathbf{D}^{b/a} \in \mathrm{SO}(3) \triangleq \{\mathbf{D} \in \mathbb{R}^{3\times3} : \mathbf{D}^{\mathrm{T}}\mathbf{D} = \mathbf{I}_3\}$, which converts vector representations as, *e.g.*, $\mathbf{v}_b = \mathbf{D}^{b/a}\mathbf{v}_a$. Finally, consider the $\mathcal{S}_b$ representations $\mathbf{v}_b \triangleq (v_1, v_2, v_3)$, $\mathbf{u}_b$, and $\mathbf{w}_b$ of $\vec{v}$, $\vec{u}$ and $\vec{w} \triangleq \vec{v} \times \vec{u}$, respectively. It holds that $\mathbf{w}_b = [\mathbf{v}_b\times]\mathbf{u}_b$, where $[\mathbf{v}_b\times] \in \mathbb{R}^{3\times3}$ is the skew-symmetric matrix Shuster (1993)

$$[\mathbf{v}_b\times] \triangleq \begin{bmatrix} 0 & -v_3 & v_2 \\ v_3 & 0 & -v_1 \\ -v_2 & v_1 & 0 \end{bmatrix}.$$

2.2 Rotor-Set Modeling

Consider the hexa-rotor and the CCSs illustrated in Fig. 1. The *ground* CCS $\mathcal{S}_g \triangleq \{G; \hat{x}_g, \hat{y}_g, \hat{z}_g\}$ is fixed to the ground at a known point G, while the *body* CCS $\mathcal{S}_b \triangleq \{B; \hat{x}_b, \hat{y}_b, \hat{z}_b\}$ is fixed to the airframe, with the origin at its center of mass B. The MAV has six fixed rotors in the following configuration: rotors 1 and 2 are parallel to $\hat{z}_b$, rotors 3 and 4 are aligned with $\hat{x}_b$, and the two last rotors are parallel to $\hat{y}_b$. Each actuator produces a thrust force and a reaction torque, which are modeled, respectively, by Mahony *et al.* (2012)

$$\vec{f}_i = k_f\omega_i^2\vec{e}_i, \tag{1}$$
$$\vec{\tau}_i = (-1)^{i+1}k_\tau\omega_i^2\vec{e}_i, \tag{2}$$

where $k_f \in \mathbb{R}_+$ and $k_\tau \in \mathbb{R}_+$ are aerodynamic coefficients, $\omega_i \in \mathbb{R}_+$ denotes the rotor's spinning rate, and $\vec{e}_i$ represents the ith rotor direction, as described above, for $i \in \{1, 2, \ldots, 6\}$.

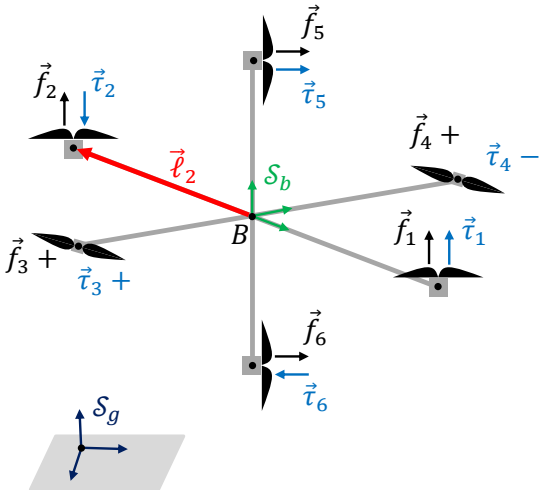

Figure 1. Schematic representation of the considered fully-actuated hexa-rotor. The black and blue arrows indicate the directions of the respective quantities.

Using the individual efforts in (1)–(2), the resulting control force and torque acting on the hexa-rotor are given,

respectively, by

$$\vec{f}^{\,c} = \sum_{i=1}^{n_r} \vec{f}_i, \tag{3}$$

$$\vec{\tau}^{\,c} = \sum_{i=1}^{n_r} \left(\vec{\ell}_i \times \vec{f}_i + \vec{\tau}_i \right), \tag{4}$$

where $\vec{\ell}_i$ is the arm vector of the ith rotor w.r.t B and is such that $\|\vec{\ell}_i\| = \ell, \forall i \in \{1, 2, \ldots, 6\}$. The $\mathcal{S}_b$ representations of the previous efforts can be expressed as

$$\mathbf{f}_b^c = \sum_{i=1}^{n_r} f_i \mathbf{e}_{i,b}, \tag{5}$$

$$\boldsymbol{\tau}_b^c = \sum_{i=1}^{n_r} f_i \left([\boldsymbol{\ell}_{i,b}\times] + k(-1)^{i+1}\mathbf{I}_3 \right) \mathbf{e}_{i,b}, \tag{6}$$

where $k \triangleq k_\tau/k_f$ and $f_i \triangleq k_f\omega_i^2$ is the magnitude of $\vec{f}_i$. Moreover, $\boldsymbol{\ell}_{i,b} \in \mathbb{R}^3$ and $\mathbf{e}_{i,b} \in \mathbb{R}^3$ are, respectively, the $\mathcal{S}_b$ representations of the vectors $\vec{\ell}_i$ and $\vec{e}_i$.

Now, assume that $\bar{\mathbf{f}}_b^c \in \mathbb{R}_+$ and $\bar{\boldsymbol{\tau}}_b^c \in \mathbb{R}^3$ are, respectively, commands for $\mathbf{f}_b^c$ and $\boldsymbol{\tau}_b^c$. Furthermore, consider that $\bar{f}_i$ is a command for f_i. Therefore, we can relate the previous commands in the same way that the respective physical quantities are related in (5)–(6), which results in the *control allocation equation*

$$\mathbf{u} = \boldsymbol{\Gamma}\bar{\mathbf{f}}, \tag{7}$$

where $\mathbf{u} \triangleq \left(\bar{\mathbf{f}}_b^c, \bar{\boldsymbol{\tau}}_b^c\right) \in \mathbb{R}^6$ is the control vector and $\bar{\mathbf{f}} \triangleq \left(\bar{f}_1, \bar{f}_2, \ldots, \bar{f}_6\right) \in \mathbb{R}^6$. Moreover, the matrix $\boldsymbol{\Gamma} \in \mathbb{R}^{6\times 6}$ is given by

$$\boldsymbol{\Gamma} \triangleq \begin{bmatrix} 0 & 0 & 1 & 1 & 0 & 0 \\ 0 & 0 & 0 & 0 & 1 & 1 \\ 1 & 1 & 0 & 0 & 0 & 0 \\ 0 & 0 & k & -k & -\ell & \ell \\ -\ell & \ell & 0 & 0 & k & -k \\ k & -k & \ell & -\ell & 0 & 0 \end{bmatrix}. \tag{8}$$

Since $\text{rank}(\boldsymbol{\Gamma}) = 6$, the considered hexa-rotor is fully-actuated. Other important consequence is that $\boldsymbol{\Gamma}$ is non-singular, thus the *control allocation* is simply calculated as

$$\bar{\mathbf{f}} = \boldsymbol{\Gamma}^{-1}\mathbf{u}, \tag{9}$$

with the rotor commands given by $\bar{\omega}_i = \sqrt{\bar{f}_i/k_f}, i \in \{1, 2, \ldots, 6\}$.

2.3 Dynamic Modeling

The dynamic equations for an arbitrary MAV can be summarized as Silva and Santos (2020)

$$\dot{\mathbf{r}}_g^{b/g} = \mathbf{v}_g^{b/g}, \tag{10}$$

$$\dot{\mathbf{v}}_g^{b/g} = \frac{1}{m}(\mathbf{D}^{b/g})^{\mathrm{T}}\mathbf{f}_b^c - g\mathbf{e}_3, \tag{11}$$

$$\dot{\mathbf{D}}^{b/g} = -\left[\boldsymbol{\omega}_b^{b/g}\times\right]\mathbf{D}^{b/g}, \tag{12}$$

$$\dot{\boldsymbol{\omega}}_b^{b/g} = \mathbf{J}_b^{-1}\boldsymbol{\tau}_b^c - \mathbf{J}_b^{-1}\left[\boldsymbol{\omega}_b^{b/g}\times\right]\left(\mathbf{J}_b\boldsymbol{\omega}_b^{b/g}\right), \tag{13}$$

where $\mathbf{r}_g^{b/g} \in \mathbb{R}^3$ and $\mathbf{v}_g^{b/g} \in \mathbb{R}^3$ are, respectively, the position and velocity of $\mathcal{S}_b$ w.r.t. $\mathcal{S}_g$, $\mathbf{D}^{b/g} \in \mathrm{SO}(3)$ represents the attitude matrix of $\mathcal{S}_b$ w.r.t. $\mathcal{S}_g$, and $\boldsymbol{\omega}_b^{b/g} \in \mathbb{R}^3$ is the angular velocity expressed in $\mathcal{S}_b$. Moreover, $m \in \mathbb{R}_+$ is the vehicle's mass, while $\mathbf{J}_b \in \mathbb{R}^{3\times 3}$ denotes its inertia matrix in system $\mathcal{S}_b$, and $g \in \mathbb{R}_+$ is the local gravity.

To model the attitude kinematics, we adopt the attitude parameterization in Gibbs vector $\boldsymbol{\sigma}^{b/g} \in \mathbb{R}^3$, which is a minimal representation of attitude and, for this reason, is more suitable to real-time implementation than the attitude matrix $\mathbf{D}^{b/g}$. The kinematics of Gibbs vector is given by (Shuster, 1993, page 484)

$$\dot{\boldsymbol{\sigma}}^{b/g} = \mathbf{M}(\boldsymbol{\sigma}^{b/g})\boldsymbol{\omega}_b^{b/g}, \tag{14}$$

where $\mathbf{M}(\boldsymbol{\sigma}) \triangleq \left(\boldsymbol{\sigma}\boldsymbol{\sigma}^{\mathrm{T}} + [\boldsymbol{\sigma}\times] + \mathbf{I}_3\right)/2$. Moreover, the conversion between this vector and the attitude matrix can be described as $\mathbf{D}^{b/g} = \mathbf{D}(\boldsymbol{\sigma}^{b/g})$, where $\mathbf{D}(\cdot)$ is the following function

$$\mathbf{D}(\boldsymbol{\sigma}) \triangleq \frac{\left(1 - \|\boldsymbol{\sigma}\|^2\right)\mathbf{I}_3 + 2\boldsymbol{\sigma}(\boldsymbol{\sigma})^{\mathrm{T}} - 2[\boldsymbol{\sigma}\times]}{1 + \|\boldsymbol{\sigma}\|^2}. \tag{15}$$

Now, we can define the vehicle's state vector as $\mathbf{x} \triangleq (\mathbf{x}_1, \mathbf{x}_2)$, with $\mathbf{x}_1 \triangleq \left(\mathbf{r}_g^{b/g}, \boldsymbol{\sigma}^{b/g}\right)$ and $\mathbf{x}_2 \triangleq \left(\mathbf{v}_g^{b/g}, \boldsymbol{\omega}_b^{b/g}\right)$. Therefore, using (10)–(11) and (13)–(14), we can derive the state equations

$$\dot{\mathbf{x}}_1 = \mathbf{g}_1(\mathbf{x}), \tag{16}$$
$$\dot{\mathbf{x}}_2 = \mathbf{g}_2(\mathbf{x}) + \mathbf{B}(\mathbf{x})\mathbf{u}, \tag{17}$$

with

$$\mathbf{g}_1(\mathbf{x}) \triangleq \begin{bmatrix} \mathbf{v}_g^{b/g} \\ \mathbf{M}(\boldsymbol{\sigma}^{b/g})\boldsymbol{\omega}_b^{b/g} \end{bmatrix}, \ \mathbf{g}_2(\mathbf{x}) \triangleq \begin{bmatrix} -g\mathbf{e}_3 \\ -\mathbf{J}_b^{-1}\left[\boldsymbol{\omega}_b^{b/g}\times\right]\left(\mathbf{J}_b\boldsymbol{\omega}_b^{b/g}\right) \end{bmatrix}, \ \mathbf{B}(\mathbf{x}) \triangleq \begin{bmatrix} \frac{1}{m}\left(\mathbf{D}^{b/g}\right)^{\mathrm{T}} & \mathbf{0}_{3\times3} \\ \mathbf{0}_{3\times3} & \mathbf{J}_b^{-1} \end{bmatrix}.$$

2.4 MAV Control Problem

Define $\bar{\mathbf{x}} \in \mathbb{R}^{12}$ as a command for the state vector $\mathbf{x}$. Using this definition, we can enunciate the problem of this paper.

Problem 1. The control problem for fully-actuated MAVs is to design a control law $\mathbf{u} = \mathbf{u}(\mathbf{x}, \bar{\mathbf{x}})$ which stabilizes the dynamics in (16)–(17) around the state command $\bar{\mathbf{x}}$.

3. CONTROL DESIGN

Consider the CCS $\mathcal{S}_{\bar{b}} \triangleq \{B; \hat{x}_{\bar{b}}, \hat{y}_{\bar{b}}, \hat{z}_{\bar{b}}\}$ as a representation of the desired orientation for $\mathcal{S}_b$. Based on this system, we can define the quantities $\bar{\mathbf{r}} \triangleq \bar{\mathbf{r}}_g^{b/g}$, $\bar{\mathbf{D}} \triangleq \mathbf{D}^{\bar{b}/g}$, $\bar{\mathbf{v}} \triangleq \bar{\mathbf{v}}_g^{b/g}$, and $\bar{\boldsymbol{\omega}} \triangleq \boldsymbol{\omega}_{\bar{b}}^{\bar{b}/g}$ as, respectively, the commands for $\mathbf{r}_g^{b/g}$, $\mathbf{D}^{b/g}$, $\mathbf{v}_g^{b/g}$, and $\boldsymbol{\omega}_b^{b/g}$. Therefore, the corresponding state errors can be defined as

$$\tilde{\mathbf{r}} \triangleq \mathbf{r}_g^{b/g} - \bar{\mathbf{r}}_g^{b/g}, \tag{18}$$
$$\tilde{\mathbf{D}} \triangleq \mathbf{D}^{b/g}\mathbf{D}^{g/\bar{b}}, \tag{19}$$
$$\tilde{\mathbf{v}} \triangleq \mathbf{v}_g^{b/g} - \bar{\mathbf{v}}_g^{b/g}, \tag{20}$$
$$\tilde{\boldsymbol{\omega}} \triangleq \boldsymbol{\omega}_b^{b/g} - \boldsymbol{\omega}_b^{\bar{b}/g}, \tag{21}$$

and the error in Gibbs vector $\tilde{\boldsymbol{\sigma}} \in \mathbb{R}^3$ is also related with $\tilde{\mathbf{D}}$ by means of (15).

The error dynamic model is derived in the following lemma.

Lemma 1. Define the state error as $\tilde{\mathbf{x}} \triangleq (\tilde{\mathbf{x}}_1, \tilde{\mathbf{x}}_2)$, with $\tilde{\mathbf{x}}_1 \triangleq (\tilde{\mathbf{r}}, \tilde{\boldsymbol{\sigma}})$ and $\tilde{\mathbf{x}}_2 \triangleq (\tilde{\mathbf{v}}, \tilde{\boldsymbol{\omega}})$. The error dynamic model is given by

$$\dot{\tilde{\mathbf{x}}}_1 = \mathbf{g}_1(\tilde{\mathbf{x}}), \tag{22}$$
$$\dot{\tilde{\mathbf{x}}}_2 = \mathbf{g}_2(\tilde{\mathbf{x}}) + \mathbf{B}(\tilde{\mathbf{x}})\mathbf{u}, \tag{23}$$

where

$$\mathbf{g}_1(\tilde{\mathbf{x}}) \triangleq \begin{bmatrix} \tilde{\mathbf{v}} \\ \mathbf{M}(\tilde{\boldsymbol{\sigma}})\tilde{\boldsymbol{\omega}} \end{bmatrix}, \mathbf{g}_2(\tilde{\mathbf{x}}) \triangleq \begin{bmatrix} -\dot{\bar{\mathbf{v}}} - g\mathbf{e}_3 \\ -\tilde{\mathbf{D}}\dot{\bar{\boldsymbol{\omega}}} + [\tilde{\boldsymbol{\omega}}\times]\tilde{\mathbf{D}}\bar{\boldsymbol{\omega}} - \mathbf{J}_b^{-1}\left[\boldsymbol{\omega}_b^{b/g}\times\right]\left(\mathbf{J}_b\boldsymbol{\omega}_b^{b/g}\right) \end{bmatrix}, \mathbf{B}(\tilde{\mathbf{x}}) \triangleq \begin{bmatrix} \frac{1}{m}\left(\mathbf{D}^{b/g}\right)^{\mathrm{T}} & \mathbf{0}_{3\times3} \\ \mathbf{0}_{3\times3} & \mathbf{J}_b^{-1} \end{bmatrix}.$$

Proof. Regarding the translational motion, from (18) and (20), we can write, respectively, that $\tilde{\mathbf{r}} = \mathbf{r}_g^{b/g} - \bar{\mathbf{r}}$ and $\tilde{\mathbf{v}} = \mathbf{v}_g^{b/g} - \bar{\mathbf{v}}$. Therefore, the time derivatives of $\tilde{\mathbf{r}}$ and $\tilde{\mathbf{v}}$ can be directly calculated using (10) and (11), which yields

$$\dot{\tilde{\mathbf{r}}} = \tilde{\mathbf{v}}, \tag{24}$$
$$\dot{\tilde{\mathbf{v}}} = \frac{1}{m}\left(\mathbf{D}^{b/g}\right)^{\mathrm{T}}\mathbf{f}_b^c - g\mathbf{e}_3 - \dot{\bar{\mathbf{v}}}. \tag{25}$$

Regarding the attitude kinematics, we first note that (12) is also valid for the attitude command $\mathbf{D}^{\bar{b}/g}$, *i.e.*, $\dot{\mathbf{D}}^{\bar{b}/g} = -[\boldsymbol{\omega}_{\bar{b}}^{\bar{b}/g}\times]\mathbf{D}^{\bar{b}/g}$. With the previous equation, (12), and (21), we can calculate the time derivative of $\tilde{\mathbf{D}}$ in (19)

$$\dot{\tilde{\mathbf{D}}} = -\left[\tilde{\boldsymbol{\omega}}\times\right]\tilde{\mathbf{D}}. \tag{26}$$

Analogously to (12) and (14), the previous equation is associated with the following kinematics in Gibbs vector

$$\dot{\tilde{\boldsymbol{\sigma}}} = \mathbf{M}(\tilde{\boldsymbol{\sigma}})\tilde{\boldsymbol{\omega}}. \tag{27}$$

Regarding the attitude dynamics, from (21), we obtain that $\tilde{\boldsymbol{\omega}} = \boldsymbol{\omega}_b^{b/g} - \tilde{\mathbf{D}}\bar{\boldsymbol{\omega}}$. Therefore, using this equation with (13) and (26), we can derive the time derivative of $\tilde{\boldsymbol{\omega}}$

$$\dot{\tilde{\boldsymbol{\omega}}} = \mathbf{J}_b^{-1}\boldsymbol{\tau}_b^c - \mathbf{J}_b^{-1}\left[\boldsymbol{\omega}_b^{b/g}\times\right]\left(\mathbf{J}_b\boldsymbol{\omega}_b^{b/g}\right) - \tilde{\mathbf{D}}\dot{\bar{\boldsymbol{\omega}}} + \left[\tilde{\boldsymbol{\omega}}\times\right]\tilde{\mathbf{D}}\bar{\boldsymbol{\omega}}. \tag{28}$$

Finally, equations (22)–(23) are obtained by considering the definitions of $\tilde{\mathbf{x}}_1, \tilde{\mathbf{x}}_2$, and rewriting (24), (25), (27), and (28) in a matrix form. □

Now, we can present the proposed control law in Theorem 1, which demonstrates the stability of the point $\tilde{\mathbf{x}} = \mathbf{0}_{12}$.

Theorem 1. Consider the control law

$$\mathbf{u} = -\mathbf{B}^{-1}(\tilde{\mathbf{x}})\left(\mathbf{A}^{\mathrm{T}}(\tilde{\mathbf{x}}_1)\mathbf{K}_1\tilde{\mathbf{x}}_1 + \mathbf{K}_2\tilde{\mathbf{x}}_2 + \mathbf{g}_2(\tilde{\mathbf{x}})\right), \tag{29}$$

where $\mathbf{K}_1 \in \mathbb{R}^{6\times6}$ and $\mathbf{K}_2 \in \mathbb{R}^{6\times6}$ are symmetric positive definite matrices, and $\mathbf{A}(\tilde{\mathbf{x}}_1) \triangleq \mathrm{diag}(\mathbf{I}_3, \mathbf{M}(\tilde{\boldsymbol{\sigma}}))$. For the closed-loop system described by (22)–(23) and (29), the equilibrium point $\tilde{\mathbf{x}} = \mathbf{0}_{12}$ is globally asymptotically stable (GAS).

Proof. The closed-loop error model is derived by replacing the control law (29) in the dynamic equations (22)–(23)

$$\dot{\tilde{\mathbf{x}}}_1 = \mathbf{g}_1(\tilde{\mathbf{x}}), \tag{30}$$

$$\dot{\tilde{\mathbf{x}}}_2 = -\mathbf{A}^{\mathrm{T}}(\tilde{\mathbf{x}}_1)\mathbf{K}_1\tilde{\mathbf{x}}_1 - \mathbf{K}_2\tilde{\mathbf{x}}_2. \tag{31}$$

For the previous system, one can easily verify that the origin is an equilibrium point.

Consider the following Lyapunov function candidate

$$V(\tilde{\mathbf{x}}) \triangleq \frac{1}{2}\tilde{\mathbf{x}}_1^{\mathrm{T}}\mathbf{K}_1\tilde{\mathbf{x}}_1 + \frac{1}{2}\tilde{\mathbf{x}}_2^{\mathrm{T}}\tilde{\mathbf{x}}_2. \tag{32}$$

Using (30)–(31), the time derivative of $V(\cdot)$ is given by

$$\dot{V}(\tilde{\mathbf{x}}) = \tilde{\mathbf{x}}_1^{\mathrm{T}}\mathbf{K}_1\mathbf{g}_1(\tilde{\mathbf{x}}) - \tilde{\mathbf{x}}_2^{\mathrm{T}}\left(\mathbf{A}^{\mathrm{T}}(\tilde{\mathbf{x}}_1)\mathbf{K}_1\tilde{\mathbf{x}}_1 + \mathbf{K}_2\tilde{\mathbf{x}}_2\right). \tag{33}$$

From (22) and (29), one can observe that $\mathbf{g}_1(\tilde{\mathbf{x}}) = \mathbf{A}(\tilde{\mathbf{x}}_1)\tilde{\mathbf{x}}_2$. Therefore, replacing this identity in (33), we obtain

$$\dot{V}(\tilde{\mathbf{x}}) = -\tilde{\mathbf{x}}_2^{\mathrm{T}}\mathbf{K}_2\tilde{\mathbf{x}}_2. \tag{34}$$

Now, consider the set $\mathcal{N} \triangleq \{\tilde{\mathbf{x}} \in \mathbb{R}^{12} : \dot{V}(\tilde{\mathbf{x}}) = 0\}$. Since function $V(\cdot)$ is radially unbounded and $\dot{V}(\cdot)$ is negative semi-definite, it can be demonstrated that the system will converge to the maximal positively invariant set $\mathcal{M} \subset \mathcal{N}$ (see Slotine and Li, 1991, Section 3.4.3). Therefore, in order to prove the global asymptotic stability of the origin, we must show that this point is the unique element of $\mathcal{M}$.

Assume an arbitrary point $\tilde{\mathbf{x}}^m \triangleq (\tilde{\mathbf{x}}_1^m, \tilde{\mathbf{x}}_2^m) \in \mathcal{M}$. Since $\mathcal{M}$ is a subset of $\mathcal{N}$, we have that $(\tilde{\mathbf{x}}_2^m)^{\mathrm{T}}\mathbf{K}_2\tilde{\mathbf{x}}_2^m = 0$, which implies that $\tilde{\mathbf{x}}_2^m = \mathbf{0}_6$. Using this point in (31), we obtain that $\dot{\tilde{\mathbf{x}}}_2^m = -\mathbf{A}^{\mathrm{T}}(\tilde{\mathbf{x}}_1^m)\mathbf{K}_1\tilde{\mathbf{x}}_1^m$. On the other hand, the set invariance of $\mathcal{M}$ implies that $\dot{\tilde{\mathbf{x}}}_2^m = \mathbf{0}_6$. Therefore, the following identity holds

$$\mathbf{A}^{\mathrm{T}}(\tilde{\mathbf{x}}_1^m)\mathbf{K}_1\tilde{\mathbf{x}}_1^m = \mathbf{0}_6. \tag{35}$$

Finally, one can show that the unique solution of the previous equation is $\tilde{\mathbf{x}}_1^m = \mathbf{0}_6$. Therefore, it results that $\mathcal{M} = \{\tilde{\mathbf{x}}^m = \mathbf{0}_{12}\}$ and this proof is completed. □

4. SIMULATION RESULTS

In order to test the proposed control law, the hexa-rotor of Fig. 1 is considered with the following parameters: $m = 0.5\,\mathrm{kg}$, $\mathbf{J}_b = 0.01\mathbf{I}_3\,\mathrm{kg\,m^2}$, $\ell = 0.25\,\mathrm{m}$, $k_f = 2.5 \times 10^{-5}\,\mathrm{kg\,m}$, and $k_\tau = 5.0 \times 10^{-7}\,\mathrm{kg\,m^2}$. Moreover, the control matrices are set as $\mathbf{K}_1 = \mathrm{diag}(\mathbf{I}_3, 3\mathbf{I}_3)$ and $\mathbf{K}_2 = 2\mathbf{I}_6$.

The proposed controller was evaluated in a waypoint tracking mission which excites all the MAV states. A waypoint $\mathbf{w}^j \in \mathbb{R}^6$ is defined as a position-attitude reference vector, with attitude expressed in Euler angles 123. The following waypoint sequence was considered (with values in SI units): $\mathbf{w}^1 = (0, 0, 10, 0, 0, 0)$, $\mathbf{w}^2 = (0, 0, 10, 0, 0, \pi/2)$, $\mathbf{w}^3 = (0, 0, 10, \pi/3, \pi/3, 0)$, $\mathbf{w}^4 = (10, 0, 10, \pi/3, \pi/3, 0)$, and $\mathbf{w}^5 = (10, 10, 10, \pi/3, \pi/3, 0)$. For each waypoint, we assumed a corresponding state command $\bar{\mathbf{x}}^j \in \mathbb{R}^{12}$ with null linear and angular velocities, *i.e.*, $\bar{\mathbf{x}}^j \triangleq (\mathbf{w}^j, \mathbf{0}_6), j \in \{1, 2, 3, 4, 5\}$. The state commands $\bar{\mathbf{x}}^j$ were passed to the control law, as step signals, at the following instants: $t_1 = 0\,\mathrm{s}$, $t_2 = 10\,\mathrm{s}$, $t_3 = 20\,\mathrm{s}$, $t_4 = 30\,\mathrm{s}$, and $t_5 = 40\,\mathrm{s}$. Moreover, at the initial time, all the vehicle's states are null.

The waypoint tracking mission was simulated in a software-in-the-loop framework, which consists in solving the MAV dynamics using MATLAB and passing the obtained states, in real-time, to a three-dimensional MAV flight simulator created by our research group. To solve the dynamic equations in (16)–(17), it was employed the Euler integrator with time step $0.01\,\mathrm{s}$. The results of this simulation are illustrated in Figs. 2–5 and we also share a video[1] of the hexa-rotor flight reproduced in real-time by our 3D simulator.

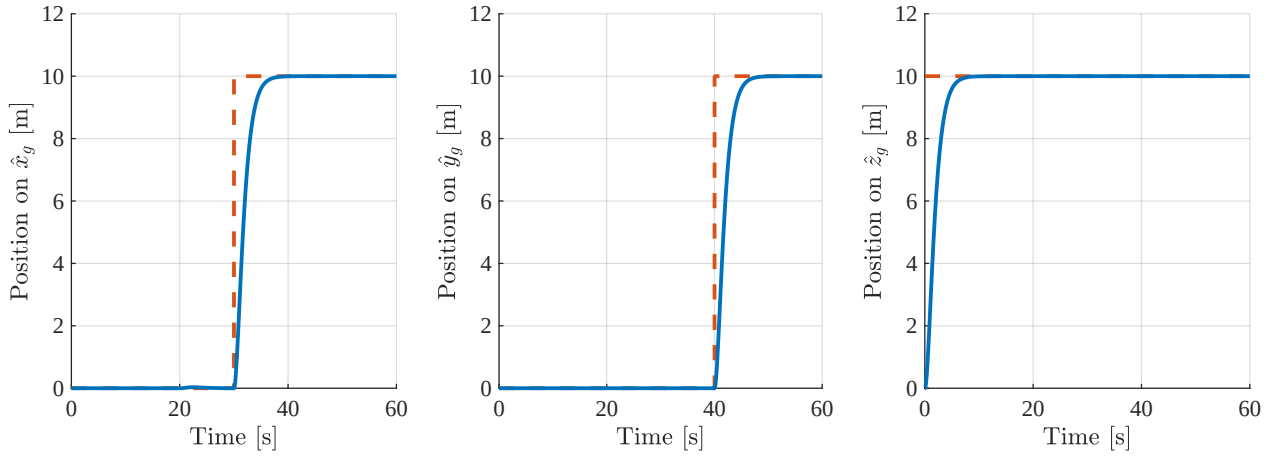

Figure 2. Position of the hexa-rotor during simulation. The physical position is illustrated by a blue line, while the commanded position is represented as a dashed red line.

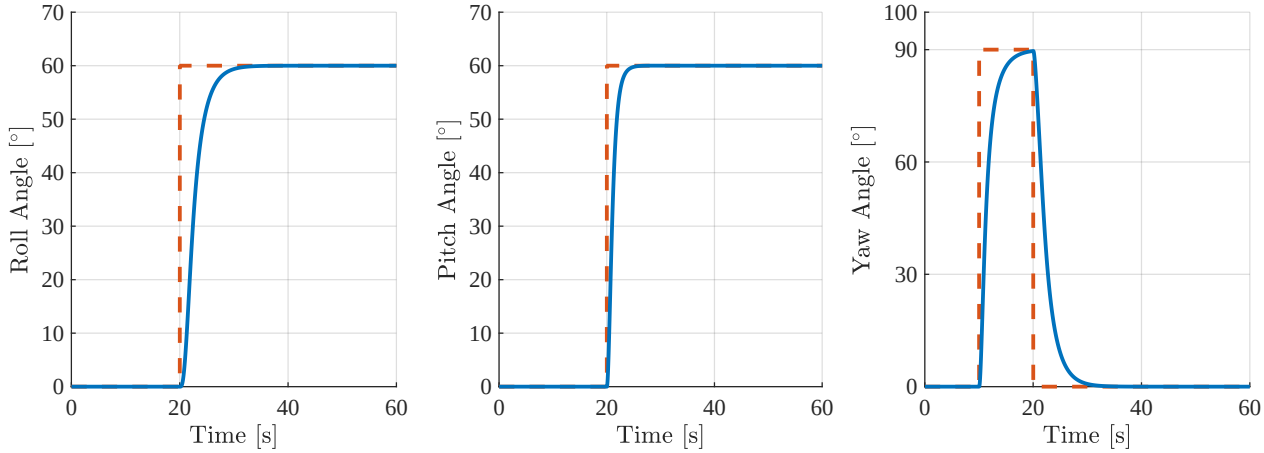

Figure 3. Attitude (in Euler angles 123) of the hexa-rotor during simulation. The physical attitude is illustrated by a blue line, while the commanded attitude is represented as a dashed red line.

The position and attitude of the hexa-rotor are presented in Figs. 2–3. For each waypoint of the sequence, we can note that the states successfully converge to the respective commands. Particularly for the waypoints $\mathbf{w}^4$ and $\mathbf{w}^5$ (which are commanded at times $30\,\mathrm{s}$ and $40\,\mathrm{s}$, respectively), we can verify that the MAV moves along the directions of $\hat{x}_g$ and $\hat{y}_g$ while the pitch and roll angles are maintained constant. On the other hand, for the third waypoint, the inverse is observed, *i.e.*, the rotation in roll and pitch do not affect the position states. These facts show features quite important for

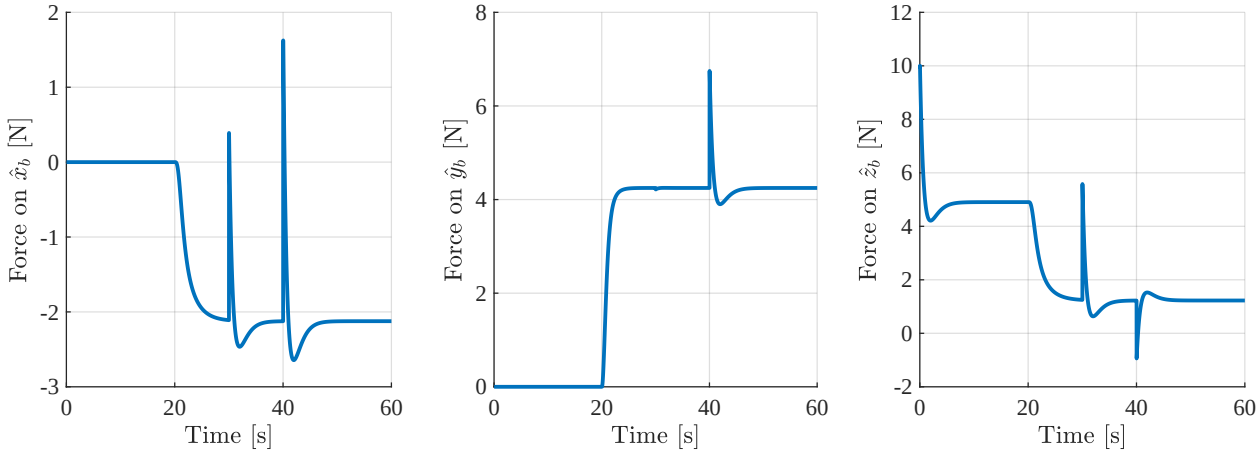

Figure 4. Force command of the proposed control law during simulation.

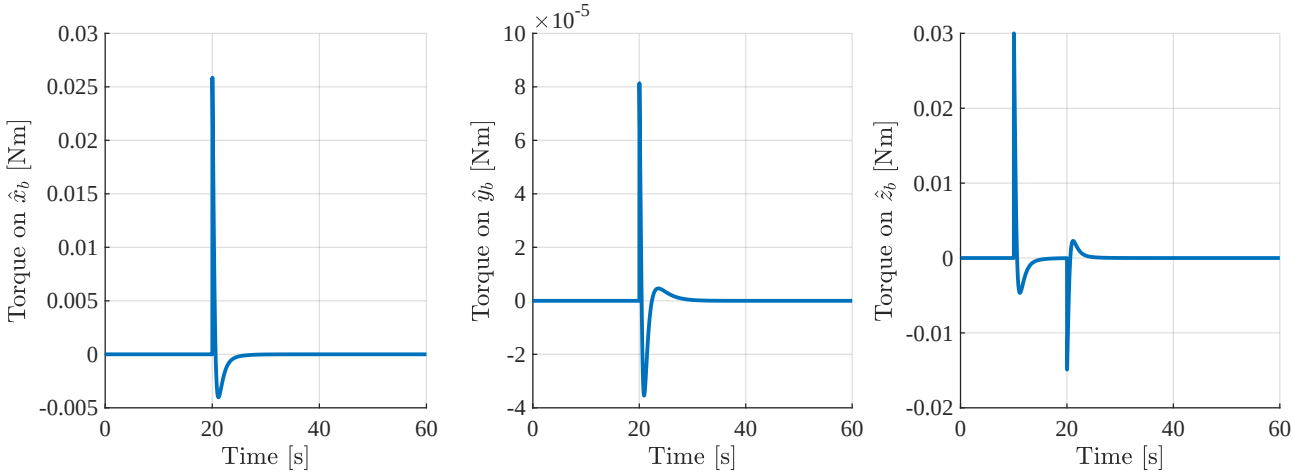

Figure 5. Torque command of the proposed control law during simulation.

fully-actuated MAVs and attest to the good performance of the proposed controller. Furthermore, using the video[1] and Figs. 4–5, we can observe that the control law did not lead the vehicle to perform abrupt moves, which are undesirable for practical applications.

5. CONCLUSION

In this paper, we have proposed a control law for fully-actuated MAVs. The proposed controller consists of an inverse-dynamic law with proportional-derivative control actions, which turns its implementation and tuning quite simple. Using the direct method of Lyapunov, we have shown that the controller provides global asymptotic stability for any state reference. Through a software-in-the-loop simulation, the flight control has been evaluated in a tracking mission with a sequence of five position-attitude waypoints. The results have demonstrated that the control law can stabilize all the hexa-rotor states, for each considered waypoint. Furthermore, the real-time simulation has shown a good control performance, which encourages the implementation of the proposed controller in automation-based applications, such as aerial manipulation and delivery of goods. Finally, as future works, we can mention: the study of a robust control law against model uncertainties and external disturbances; and the application of the proposed control law in an experiment using a fully-actuated MAV prototype.

6. ACKNOWLEDGEMENTS

The authors would like to thank the São Paulo Research Foundation (FAPESP), for the financial support under grant 2019/05334-0. The first author also thanks to the Brazilian Air Force for the educational and professional support. The second author is also grateful for the support of the Brazilian National Council for Scientific and Technological Development (CNPq), under grant 302637/2018-4.

[1] https://drive.google.com/file/d/1OcOeYATr71CjsPJvtwM9lzb4rzBprSc0/view?usp=sharing

7. REFERENCES

Brescianini, D. and D'Andrea, R., 2016. "Design, modeling and control of an omni-directional aerial vehicle". In *2016 IEEE International Conference on Robotics and Automation (ICRA)*. pp. 3261–3266. doi: 10.1109/ICRA.2016.7487497.

Crowther, B., Lanzon, A., Maya-Gonzalez, M. and Langkamp, D., 2011. "Kinematic analysis and control design for a nonplanar multirotor vehicle". *Journal of Guidance, Control, and Dynamics*, Vol. 34, No. 4, pp. 1157–1171. doi: 10.2514/1.51186.

Diógenes, H.B. and Santos, D.A., 2017. "Dynamic modeling and control of a quadcopter with longitudinal-tilting rotors". In *XXXVIII Iberian Latin American Congress on Computational Methods in Engineering*. doi: 10.20906/cps/cilamce2017-1157.

Franchi, A., Carli, R., Bicego, D. and Ryll, M., 2018. "Full-pose tracking control for aerial robotic systems with laterally bounded input force". *IEEE Transactions on Robotics*, Vol. 34, No. 2, pp. 534–541. doi:10.1109/TRO.2017.2786734.

Hua, M.D., Hamel, T., Morin, P. and Samson, C., 2015. "Control of vtol vehicles with thrust-tilting augmentation". *Automatica*, Vol. 52, pp. 1 – 7. ISSN 0005-1098. doi:https://doi.org/10.1016/j.automatica.2014.10.129.

Invernizzi, D. and Lovera, M., 2017. "Geometric tracking control of a quadcopter tiltrotor uav". *IFAC-PapersOnLine*, Vol. 50, No. 1, pp. 11565 – 11570. ISSN 2405-8963. doi:https://doi.org/10.1016/j.ifacol.2017.08.1645. 20th IFAC World Congress.

Kamel, M., Verling, S., Elkhatib, O., Sprecher, C., Wulkop, P., Taylor, Z., Siegwart, R. and Gilitschenski, I., 2018. "The voliro omniorientational hexacopter: An agile and maneuverable tiltable-rotor aerial vehicle". *IEEE Robotics Automation Magazine*, Vol. 25, No. 4, pp. 34–44. doi:10.1109/MRA.2018.2866758.

Mahony, R., Kumar, V. and Corke, P., 2012. "Multirotor aerial vehicles: Modeling, estimation, and control of quadrotor". *IEEE Robotics Automation Magazine*, Vol. 19, No. 3, pp. 20–32. doi:10.1109/MRA.2012.2206474.

Oosedo, A., Abiko, S., Narasaki, S., Kuno, A., Konno, A. and Uchiyama, M., 2016. "Large attitude change flight of a quad tilt rotor unmanned aerial vehicle". *Advanced Robotics*, Vol. 30, No. 5, pp. 326–337. doi: 10.1080/01691864.2015.1134344.

Park, S., Her, J., Kim, J. and Lee, D., 2016. "Design, modeling and control of omni-directional aerial robot". In *2016 IEEE/RSJ International Conference on Intelligent Robots and Systems (IROS)*. pp. 1570–1575. doi: 10.1109/IROS.2016.7759254.

Rajappa, S., Ryll, M., Bülthoff, H.H. and Franchi, A., 2015. "Modeling, control and design optimization for a fully-actuated hexarotor aerial vehicle with tilted propellers". In *2015 IEEE International Conference on Robotics and Automation (ICRA)*. pp. 4006–4013. doi:10.1109/ICRA.2015.7139759.

Ryll, M., Bicego, D. and Franchi, A., 2016. "Modeling and control of fast-hex: A fully-actuated by synchronized-tilting hexarotor". In *2016 IEEE/RSJ International Conference on Intelligent Robots and Systems (IROS)*. pp. 1689–1694. doi:10.1109/IROS.2016.7759271.

Ryll, M., Bicego, D., Giurato, M., Lovera, M. and Franchi, A., 2020. "Fast-hex – a morphing hexarotor: Design, mechanical implementation, control and experimental validation". Preprint.

Ryll, M., Bülthoff, H.H. and Giordano, P.R., 2012. "Modeling and control of a quadrotor uav with tilting propellers". In *2012 IEEE International Conference on Robotics and Automation*. pp. 4606–4613. doi:10.1109/ICRA.2012.6225129.

Santos, D.A., Saotome, O. and Cela, A., 2013. "Trajectory control of multirotor helicopters with thrust vector constraints". In *21st Mediterranean Conference on Control and Automation*. pp. 375–379. doi:10.1109/MED.2013.6608749.

Segui-Gasco, P., Al-Rihani, Y., Shin, H.S. and Savvaris, A., 2013. "A novel actuation concept for a multi rotor uav". In *2013 International Conference on Unmanned Aircraft Systems (ICUAS)*. pp. 373–382. doi: 10.1109/ICUAS.2013.6564711.

Shuster, M.D., 1993. "A Survey on Attitude Representations". *Journal of the Astronautical Sciences*, Vol. 41, No. 4, pp. 439–517.

Silva, A.L. and Santos, D.A., 2020. "Fast nonsingular terminal sliding mode flight control for multirotor aerial vehicles". *IEEE Transactions on Aerospace and Electronic Systems*, Vol. 56, No. 6, pp. 4288 – 4299. doi: 10.1109/TAES.2020.2988836.

Slotine, J. and Li, W., 1991. *Applied Nonlinear Control*. Prentice-Hall International Editions. Prentice-Hall. ISBN 9780130400499.

8. RESPONSIBILITY NOTICE

The authors are solely responsible for the printed material included in this paper.